Mon. Not. R. Astron. Soc. **364,** 1041–1053 (2005) doi:10.1111/j.1365-2966.2005.09638.x

Molecular hydrogen and [Fe II] in active galactic nuclei – II. Results for Seyfert 2 galaxies

A. Rodríguez-Ardila,[1]★† R. Riffel[2] and M. G. Pastoriza[2]

[1]*Laboratório Nacional de Astrofísica/MCT - Rua dos Estados Unidos 154, Bairro das Nações. CEP 37504-364, Itajubá, MG, Brazil*
[2]*Departamento de Astronomia, Universidade Federal do Rio Grande do Sul. Av. Bento Gonçalves 9500, Porto Alegre, RS, Brazil*

Accepted 2005 September 22. Received 2005 September 20; in original form 2005 April 18

ABSTRACT

Near-infrared spectroscopy is used to study the kinematics and excitation mechanisms of H_2 and [Fe II] lines in a sample dominated by Seyfert 2 galaxies. The spectra simultaneously cover the *JHK* bands, allowing us to compare line fluxes emitted in the interval 0.8–2.4 μm and avoiding aperture and seeing effects. The H_2 lines are systematically narrower than the narrow-line region lines, suggesting that, very likely, the H_2 does not originate from the same parcel of gas that forms the narrow-line region. Emission-line ratios between H_2 lines favour thermal excitation mechanisms for the molecular gas in active galactic nuclei. It was found that non-thermal excitation contributes, at most, 30 per cent of the observed H_2. Thermal excitation is also confirmed by the rather similar vibrational and rotational temperatures in the objects ($\sim$2000 K). The mass of hot H_2 ranges from 10^2 to 10^3 $M_\odot$, with nearly half of objects showing values of $<$500 $M_\odot$. It shows that the fraction of molecular mass present in the nuclear region and emitting in the near-infrared is a very small fraction of the warm molecular mass present in the centre. A diagnostic diagram composed of the line ratios $H_2/Br\gamma$ and [Fe II]/Paβ proves to be a useful tool in the near-infrared for separating emission-line objects by their degree of nuclear activity. We found that active galactic nuclei are characterized by H_2 2.121 μm/Brγ and [Fe II] 1.257 μm/Paβ flux ratios between 0.6 and 2. Starburst/H II galaxies display line ratios $<$0.6 while low-ionization nuclear emission-line regions are characterized by values larger than 2 in either ratio.

Key words: line: formation – molecular processes – galaxies: Seyfert – infrared: galaxies.

1 INTRODUCTION

One important challenge in the understanding of the physics of emission-line galaxies is explaining the presence of molecular lines in the inner few hundred parsec from the central source. These lines are detected in galaxies displaying varying degrees of nuclear activity, from objects classified as starburst dominated to those classified as active galactic nucleus (AGN) dominated. Of particular importance are the latter group of sources, where unification models (Antonucci & Miller 1985) predict the presence of a molecular torus that obscures the view of the central source under some orientation angles. This would be the cause of the different classes of AGNs observed (Seyfert 1, Seyfert 2, blazars, etc.). Because of the large optical depth A_V that such a torus requires, it would serve as a natural reservoir of molecular gas, protecting it from being destroyed by the intense and hard radiation field from the central source. It has also been suggested that the torus is likely responsible for the molecular emission lines often detected in the spectra of AGNs. In fact, Alloin & Galliano (2002) and Gratadour et al. (2003), for instance, using subarcsec spectroscopy on NGC 1068, found evidence of a disc of H_2 on scales of a few tens of parsec, related to the putative torus of the unified model.

Alternatively, in the last few years, large efforts have been devoted to the study of composite objects, those where a circumnuclear starburst coexists with a low-luminosity AGN (Ivanov et al. 2000; Contini et al. 2002; Sturm et al. 2002). If a burst of star formation is taking place or occurred very recently, the presence of molecular clouds associated with star-forming regions will leave spectral signatures that contaminate the AGN spectrum. Therefore, whether the H_2 lines observed in AGNs are directly associated with either the molecular torus or the circumnuclear star formation remains an open question. It is also possible that the molecular gas is directly associated with the AGN, but distributed in the circumnuclear region, on scales of a few hundred of parsec. In this case, the excitation of the molecular gas can be due to more than one process. Shocks by radio jets and X-ray heating, for instance, are plausible mechanisms that

★Visiting Astronomer at the Infrared Telescope Facility, which is operated by the University of Hawaii under Cooperative Agreement no. NCC 5-538 with the National Aeronautics and Space Administration, Office of Space Science, Planetary Astronomy Program.

†E-mail: aardila@lna.br

have been suggested on observational grounds (Knop et al. 1996; Reunanen, Kotilainen & Prieto 2002).

The H_2 lines may be produced by three types of excitation mechanisms: ultraviolet (UV) fluorescence (Black & van Dishoeck 1987), also known as non-thermal excitation; shocks (Hollenbach & McKee 1989); X-ray illumination (Maloney, Hollenbach & Tielens 1996). The latter two are often referred to as thermal processes. Each of these three processes produces a different spectrum, and the relative intensities between emission lines of H_2 can be used to discriminate among them.

Very recently, Rodríguez-Ardila et al. (2004, hereafter Paper I) carried out a pioneer study of the excitation mechanisms leading to the emission of H_2 in a sample composed mostly of Seyfert 1 galaxies. They detected lines of that molecule in 90 per cent of their sample, showing that hot H_2 ($T \sim 2000$ K) is present in almost all AGNs, including quasars. In addition, they concluded that the dominant excitation mechanism of the H_2 lines is thermal, with a clear contribution of processes associated to the nuclear source. A clear advantage of Paper I over similar works published in the past (Larkin et al. 1998; Rigolopoulou et al. 2002) is that the integrated spectra cover the inner 300 pc in most objects of the sample, minimizing contamination introduced by the host galaxy.

In addition to the excitation mechanisms leading to H_2 in AGNs, it is also interesting to study the processes that are responsible of the [Fe II] emission. This is because usually [Fe II] and H_2 are suggested to be formed in the same parcel of gas and closely associated with star-forming regions. However, evidence accumulated over the past years shows that in AGNs [Fe II] can have different sources but, very likely, these are all directly related to the central engine (Forbes & Ward 1993; Goodrich, Veilleux & Hill 1994; Simpson et al. 1996; Alonso-Herrero et al. 1997; Mouri, Kawara & Taniguchi 2000).

Here, we continue the study of the excitation mechanisms leading to the emission of H_2 and [Fe II] for a sample of AGNs, most of them near enough to allow us to map the molecular emission at scales of ∼200 pc (64 per cent of the objects) and to scales down to 300 pc for 82 per cent of the galaxies. In addition, the spectra were acquired with the same instrumentation employed in Paper I, with simultaneous observations of the *JHK* bands, eliminating differences in aperture and seeing variations across the bands. This represents an improvement over previous works (Veilleux, Goodrich & Hill 1997a; Larkin et al. 1998; Reunanen, Kotilainen & Prieto 2002, 2003) because of the large wavelength coverage and the number of diagnostic lines observed. To our knowledge, the H_2 and [Fe II] measurements reported here and in Paper I constitute the most complete and homogeneous set of data for a sample of AGNs.

Paper I showed that the diagnostic diagram H_2 2.121 μm/Brγ versus [Fe II] 1.257 μm/Paβ, proposed by Larkin et al. (1998), is an efficient tool in the near-infrared (NIR) to separate emission-line objects by the level of nuclear activity. The inclusion of a new set of objects will allow us to fine-tune and test the confidence of the diagram as a useful tool to classify a large sample of objects by the level of nuclear activity.

This paper is structured as follows. In Section 2 we present the observations and data reduction. In Section 3 we discuss the kinematics of the molecular and [Fe II] gas inferred from their line profiles. In Section 4 we discuss the excitation mechanisms of the H_2 lines in AGNs. In Section 5 we analyse the line ratios H_2 2.121 μm/Brγ and [Fe II] 1.257 μm/Paβ for different emission-line objects and the apparent correlation between these ratios over a large range of values. We also discuss the physical processes that drive the emission of H_2 and [Fe II] according to the values measured from the line ratios. Concluding remarks are given in Section 6. A Hubble constant of 75 km s^{-1} Mpc^{-1} is used throughout this work.

2 OBSERVATIONS AND DATA REDUCTION

NIR spectra in the interval 0.8–2.4 μm were obtained at the National Aeronautics and Space Administration (NASA) 3-m Infrared Telescope Facility (IRTF) on 2003 October 23–24 and 2004 June 01–02 with the SpeX spectrometer (Rayner et al. 2003). The detector consisted of a 1024 × 1024 ALADDIN 3 InSb array with a spatial scale of 0.15 arcsec pixel^{-1}. Simultaneous wavelength coverage was obtained by means of prism cross-dispersers. A 0.8 × 15 arcsec^2 slit was used during the observations, giving a spectral resolution of 360 km s^{-1}. This value was determined both from the arc lamp and the arc line spectra, and was found to be constant with wavelength within 3 per cent. The slit was aligned to the parallactic angle in order to minimize slit loses because of differential refraction. During the different nights, the seeing varied between 0.7 and 1 arcsec. Observations were performed nodding in an ABBA source pattern with typical individual integration times of 120–180 s and total on-source integration times between 35 and 50 min. For some sources, we took spectra on subsequent nights which were, after reduction, combined to form a single spectrum. During the observations, A0 V stars were observed near each target to provide telluric standards at similar airmasses. They were also used to flux calibrate the sample. Table 1 shows the log of the observations. The galaxies are listed in order of right ascension.

The spectral extraction and wavelength calibration procedures were performed using SPEXTOOL, the in-house software developed and provided by the SpeX team for the IRTF community (Cushing, Vacca & Rayner 2004),[1] following the same procedures as described in Paper I. Column 10 of Table 1 lists the radius of the integrated region, in parsec, with centre at the peak of the continuum light distribution for every object of the sample. As in Paper I, no effort was made to extract spectra at positions different from the nuclear region, even though some objects show evidence of extended emission. Telluric absorption correction and flux calibration was applied to the individual one-dimensional spectra by means of the IDL-based routine XTELLCOR (Vacca, Cushing & Rayner 2003).

The one-dimensional wavelength and flux-calibrated spectra were then corrected for redshift, determined from the average z measured from the position of [S III] 0.953 μm, Paδ, He I 1.083 μm, Paβ and Brγ. Finally, a Galactic extinction correction was applied, as determined from the *COBE*/*IRAS* infrared maps of Schlegel, Finkbeiner & Davis (1998). The value of the Galactic $E(B-V)$ used for each galaxy is listed in column 5 of Table 1. Final reduced spectra, in the spectral regions of interest in this work, are plotted in Figs 1–4.

3 KINEMATICS OF THE H_2 AND [FE II] LINES

The main goal of this section is to discuss how the width of H_2 2.1213 μm compares to that of other narrow lines. This will allow us to set important constrains about the location of the molecular gas. In

[1] SPEXTOOL is available from the IRTF website at http://irtfweb.ifa.hawaii.edu/∼spex/.

Table 1. Observation log and basic galactic properties for the sample.

ID	Galaxy	Type	z	$E(B-V)_G$ (mag)	Date of observation	Exposure time (s)	Airmass	PA deg	r (pc)[a]
(1)	(2)	(3)	(4)	(5)	(6)	(7)	(8)	(9)	(10)
1	Mrk 334	Sy1	0.021956	0.047	2003 Oct 23	16×120	1.00	303	340
2	NGC 34	Sy2	0.019784	0.027	2003 Oct 24	14×120	1.19	0	230
3	NGC 262	Sy2	0.015034	0.067	2003 Oct 24	10×120	1.03	160	175
4	Mrk 993	Sy2	0.015537	0.060	2003 Oct 23	16×120	1.03	160	241
5	NGC 591	Sy2	0.015167	0.046	2003 Oct 24	12×150	1.05	160	206
6	Mrk 573	Sy2	0.017259	0.023	2003 Oct 24	12×150	1.10	40	267
7	NGC 1097	Sy1	0.004253	0.027	2003 Oct 23	12×60	1.6	0	58
8	NGC 1144	Sy2	0.028847	0.072	2003 Oct 24	10×150	1.09	27	447
9	Mrk 1066	Sy2	0.012025	0.132	2003 Oct 23	16×120	1.07	146	186
10	NGC 1275	Sy2	0.017559	0.163	2003 Oct 23	12×120	1.16	135	272
11	NGC 1614	Sy2	0.015938	0.154	2003 Oct 24	12×150	1.14	0	154
12	MCG–5–13–17	Sy1	0.012642	0.017	2003 Oct 23	12×120	1.65	0	196
					2003 Oct 24	10×120	1.69	0	196
13	NGC 2110	Sy2	0.007789	0.375	2003 Oct 23	12×120	1.14	20	121
					2003 Oct 24	8×150	1.14	20	121
14	ESO428-G014	Sy2	0.005664	0.197	2003 Oct 24	8×120	1.56	345	88
15	NGC 5929	Sy2	0.008312	0.024	2004 Jun 01	14×120	1.38	116	193
16	NGC 5953	Sy2	0.006555	0.049	2004 Jun 02	12×180	1.18	0	165
17	Arp 102B	Sy1	0.024167	0.024	2004 Jun 02	16×180	1.22	0	702
18	Ark 564	Sy1	0.024684	0.060	2003 Oct 24	18×120	1.05	250	382
19	NGC 7469	Sy1	0.016317	0.069	2003 Oct 23	16×120	1.03	303	253
20	NGC 7674	Sy2	0.028924	0.059	2003 Oct 23	18×120	1.02	303	448
21	NGC 7682	Sy2	0.017125	0.067	2003 Oct 24	20×120	1.06	314	179
22	NGC 7714	H II	0.009333	0.052	2003 Oct 24	20×120	1.05	348	114

[a]Radius of the integrated region.

Paper I we already found, for a sample of mostly Seyfert 1 galaxies, that H_2 2.1213 μm was spectroscopically unresolved or with FWHM systematically narrower than that of the forbidden lines associated with the narrow-line region (NLR). This was interpreted in terms of a kinematical disconnection between the molecular and NLR gas. It is important to check if that result also holds for Seyfert 2s. Previous results are controversial. Imaging of H_2 emission carried out by Quillen et al. (1999) on a sample of Seyfert galaxies found H_2 on scales of a few hundred parsec from the nucleus. In sources such as NGC 5643, NGC 2110 and Mrk 1066, the H_2 emission was found to be coincident with [O III] and Hα+[N II], suggesting that the molecular gas may follow the NLR gas. In contrast, in NGC 3227, they found that the molecular emission originates in a 100-pc diameter disc that is not directly associated with either the [O III] emission or the 18-cm radio emission. This last result is additionally supported by observations of Schinnerer, Eckart & Tacconi (1999), who suggest that the molecular gas in NGC 3727, as well as that in NGC 1068, is distributed in a warp disc with a radius as small as 75 pc. With our data, a relationship between the kinematics of the molecular and NLR gas can be examined by comparing the emission-line profiles of H_2 and those emitted by the NLR. Note that we have implicitly assumed that the widths of the NLR lines reflect the large-scale motions of the emitting clouds in the gravitational potential of the central mass. As a result, similar widths between molecular and forbidden lines suggest that they are co-spatial.

Table 2 lists the intrinsic FWHM, in km s^{-1}, found for [S III] 0.9531 μm, [Si VI] 1.963 μm, [Fe II] 1.2567 μm and H_2 1.957, 2.0332 and 2.121 μm. The error associated with the FWHM is dominated by the uncertainty in the placement of the continuum and is ∼30 km s^{-1}. A line was consider to be spectroscopically resolved if its measured FWHM was larger than 500 km s^{-1}. This value warrants that the intrinsic FWHM is equal or larger than the instrumental one (360 km s^{-1}), after correction (in quadrature) for this effect. This means that lines with FWHM equal to 360 km s^{-1} in Table 2 may have measured FWHM values between 360 and 499 km s^{-1}. They are considered unresolved because their intrinsic width is smaller or equal to the instrumental one. Fig. 5 compares the observed line profiles of [Fe II] 1.257 μm (full histogram) and that of H_2 2.122 μm (dashed histogram) for a subsample of the objects listed in Table 2. An inspection of the figure allows us to say that [Fe II] tends to be broader than H_2, including the two galaxies common to the Quillen et al. (1999) sample (NGC 2110 and Mrk 1066). In NGC 34 and Arp 102B, both profiles are rather similar; however, these two targets are not genuine Seyfert galaxies but objects with low-ionization nuclear emission-line region (LINER)/Seyfert characteristics.

It is easy to see that the gas velocities derived for [Fe II] and H_2, listed in Table 2, follow a similar trend to that found in Paper I, although some differences are noted. In the present work, for example, H_2 (1,0) S(1) is spectroscopically resolved in 20 per cent of the objects (maximum FWHM values around 430 km s^{-1}) while in Paper I it was at the limit of the spectral resolution (360 km s^{-1}) in all sources. Similarly, [Fe II] is resolved in 68 per cent of the sample (with maximum FWHM value of 710 km s^{-1}) versus the 50 per cent resolved in Paper I (FWHM values of up to 650 km s^{-1}). Also, [S III] 0.953 μm is resolved in all AGNs except in NGC 7714, with the largest value found in NGC 1275 (FWHM = 1340 km s^{-1}). In Paper I, it was resolved in only 40 per cent of the objects, with FWHM values reaching 865 km s^{-1} (Mrk 1239). In spite of these differences, the distribution of FWHM values for Seyfert 1s and 2s are rather similar, as can be checked in Fig. 6, where the distribution of FWHM for [Fe II] 1.257 μm (upper panel), H_2 2.121 μm (middle panel) and [S III] 0.953 μm (bottom panel) are plotted.

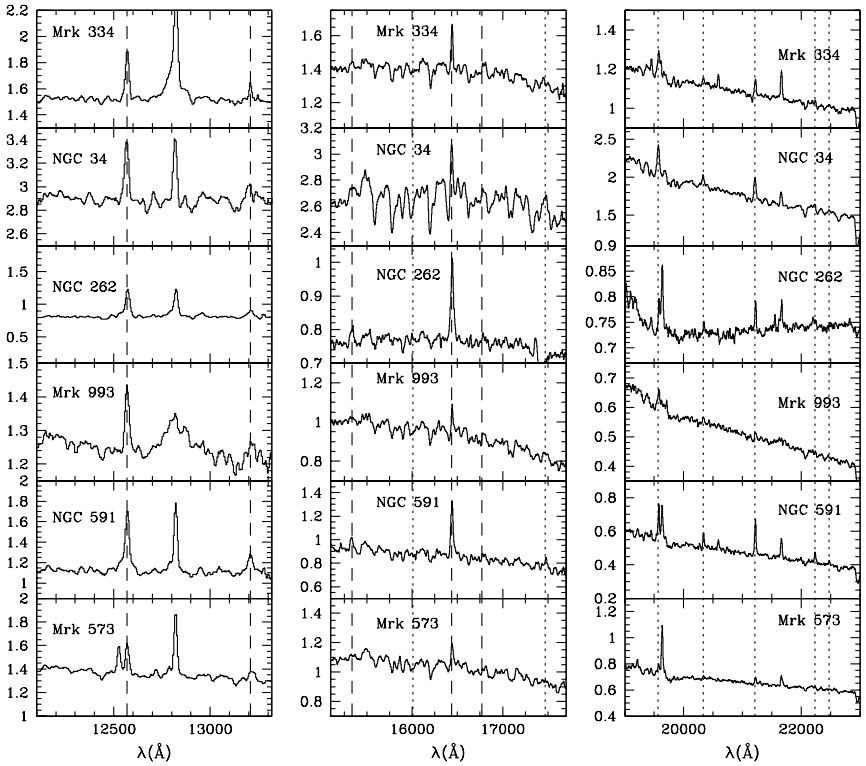

Figure 1. Final reduced spectra in the Earth's frame. For each object, the left panel is centred near Paβ, the middle panel corresponds to the *H* band spectrum, and the right panel shows the *K* band spectrum. The abscissa is the observed flux in units of 10^{-15} erg cm^{-2} s^{-1} Å^{-1}. The identified [Fe II] (dashed line) and H_2 (dotted lines) are marked in the spectra.

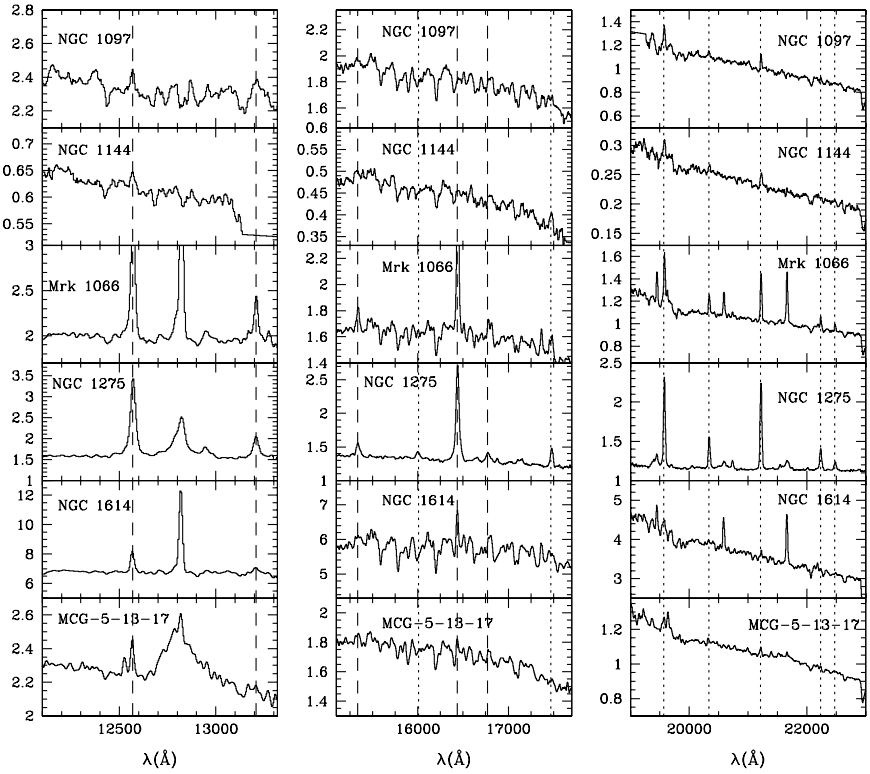

Figure 2. Same as Fig. 1.

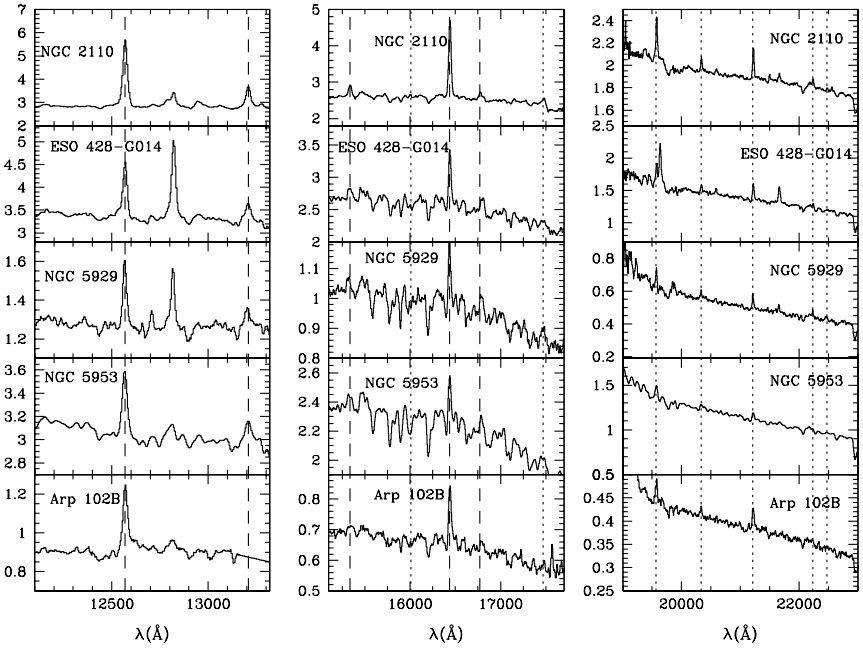

Figure 3. Same as Fig. 1.

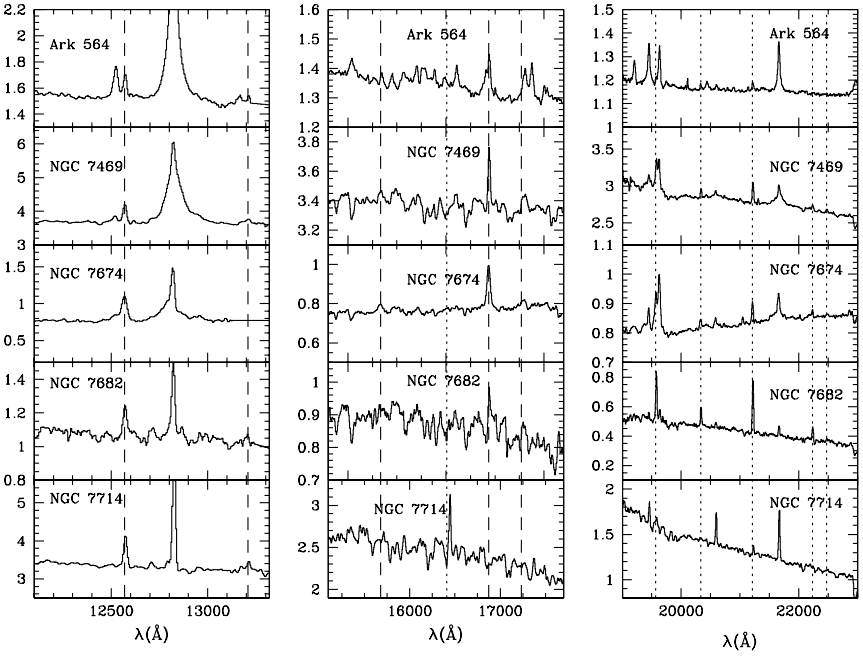

Figure 4. Same as Fig. 1.

While the velocity distribution for the former and the latter ions is similar in both Seyfert 1s (full histogram) and Seyfert 2s (dashed histogram), spanning a large range of velocities (from 360 to ∼700 km s^{-1}), 84 per cent of galaxies show H_2 lines that are not resolved spectroscopically, with only a few objects displaying values of up to 450 km s^{-1}. Note that Fig. 6 includes the FWHM found in Paper I and this work.

Fig. 6 strongly suggests that H_2 is kinematically disconnected from the NLR gas. It can be argued that the difference in linewidth is related to the fact that the H_2 lines are formed in the outer portions of the NLR, up to distances of nearly 1 kpc. However, previous works carried out with samples containing a smaller number of objects (Reunanen et al. 2002, 2003) found large concentrations of molecular gas in the nucleus, regardless of the Seyfert type. Moreover, the sizes of the nuclear H_2 emission derived from the work of Reunanen et al. vary from <20 to ∼300 pc, which is rather similar to the size of the integrated region covered by our spectra (see column 10 of Table 1, for instance). Rotation curves for H_2 also derived

Table 2. FWHM (in km s^{-1}), corrected for instrumental resolution (this correction was applied to lines with FWHM > 550 km s^{-1} and lines with smaller values are reported as unresolved, i.e. with FWHM = 360 km s^{-1}), for H_2 and other important lines measured in the sample.

Galaxy	[Si VI] (1.964)	[Fe II] (1.257)	H_2 (1.957)	H_2 (2.0332)	H_2 (2.121)	[S III] (0.9530)
Mrk 334	–	380	360[a]	375	360	610
NGC 34	–	500	430[a]	365	430	440
NGC 262	360	515	360	360	360	540
Mrk 993	–	475	360	430	370	640
NGC 591	390	620	360	360	360	525
Mrk 573	360	395	360	–	360	435
NGC 1097	–	–	365	400	415	–
NGC 1144	–	–	–	360	390	520
Mrk 1066	360	440	360	360	360	505
NGC 1275	–	710	390	395	375	1340
NGC 1614	–	440	360	–	360	440
MCG–05–13–017	575	375	415[a]	–	415	420
NGC 2110	–	575	360	360	360	670
ESO 428-G014	385	470	360	360	360	525
NGC 5929	–	450	360	360	360	405
NGC 5953	–	610	550[b]	500	440	680
Arp 102B	–	675	430	360	395	715
ARK 564	420	390	360	360	360	635
NGC 7469	360	390	490[b]	360	360	645
NGC 7674	745	660	360	380	360	400
NGC 7682	360	460	360	360	360	425
NGC 7714	–	360	–	–	360	380

[a]The line was constrained to have the same width as that of H_2 2.121 μm. [b]Strongly affected by telluric absorption.

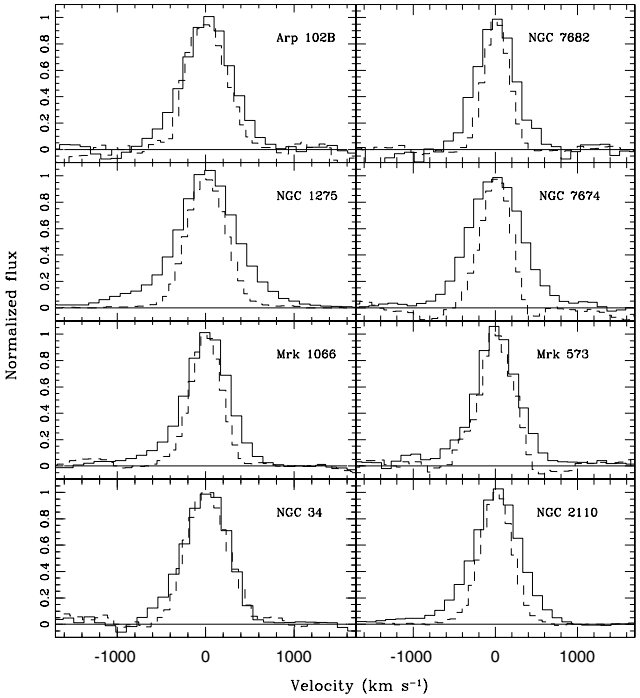

Figure 5. Comparison of the line profiles of [Fe II] 1.257 μm (full histogram) and H_2 2.122 μm (dashed histogram) for a subsample of objects.

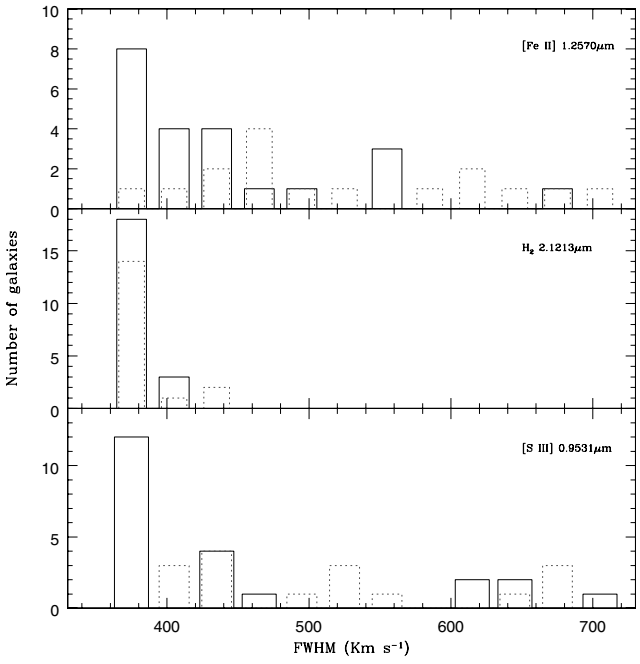

Figure 6. Histogram showing the FWHM distribution for the Seyfert 1 (full line) and Seyferts 2 (dashed lines) galaxies of this paper (see Table 2) and Paper I. The upper panel displays the results for [Fe II] 1.257 μm, the middle panel those obtained for H_2 2.122 μm and the bottom panel the distribution for [S III] 0.953 μm.

by Reunanen et al. (2002, 2003) support this disconnection. They found that the H_2 gas is most probably arranged in a disc surrounding the nucleus. This morphology would not be observed in [Fe II] and Brγ.

In summary, the observational evidence presented here confirms that H_2 is common within the inner few hundred parsec of an AGN, regardless its type. However, the molecular gas follows a different kinematics than that of the classical NLR gas, as can be inferred

from the large differences in linewidth between the molecular lines and that of the NLR. Rotation curves derived for H_2 and published by Reunanen et al. (2002, 2003) on objects that are common to our sample support this hypothesis and point to a scenario where a disc of H_2 surrounds the nuclear region.

4 EXCITATION MECHANISMS OF THE NEAR-INFRARED H_2 LINES

Three distinct mechanisms have been pointed out for the excitation of the H_2 molecule: (i) UV fluorescence, where photons in the Lyman–Werner band (912–1108 Å) are absorbed by H_2 and then re-emitted, resulting in the population of the various vibration–rotational levels of the ground electronic state (see, for example, Black & van Dishoeck 1987); (ii) shocks, where high-velocity gas motions heat, chemically alter and accelerate the ambient gas resulting in excitation of the H_2 molecule (see, for example, Hollenbach & McKee 1989); (iii) X-ray illumination, where hard X-ray photons penetrate deep into molecular clouds, heating large amounts of molecular gas resulting in H_2 emission (see, for example, Maloney et al. 1996). Each of these three mechanisms (the first usually termed as non-thermal with the latter two as thermal) produces a different H_2 spectrum; therefore, the relative intensities between emission lines of H_2 can help to discriminate the dominant excitation process. Note that an alternative to process (iii) is that the molecular gas is heated by exposure to UV photons instead of X-ray radiation. This is usually the case of dense, static photodissociation regions (PDRs; Sternberg & Dalgarno 1989).

Columns 5–9 of Table 3 list the fluxes of the most important H_2 lines detected in the *K* band (H_2 1.957 μm, 2.0332 μm, 2.1213 μm, 2.223 μm and 2.247 μm, respectively). Although other H_2 lines may be present in the spectra (in the *H* band, for instance), our interest in those listed in Table 3 is that they were proposed by Mouri (1994) as useful diagnostics for the determination of the dominant excitation mechanism of H_2. In order to discriminate between thermal and non-thermal excitation, Mouri (1994) asserted that the line ratio H_2 (1,0) S(2) 2.247 μm/(1,0) S(1) 2.212 μm separates thermal-dominated gas (with $I_{2.247\ \mu m}/I_{2.212\ \mu m} \sim 0.1$–$0.2$) from fluorescent-dominated gas (with $I_{2.247\ \mu m}/I_{2.212\ \mu m} \sim 0.55$). Moreover, the ratio H_2 (1,0) S(2) 2.033 μm/(1–0) S(0) 2.223 μm helps in determining the thermal excitation temperature. Note that in dense gas ($n \geqslant 10^4$ cm^{-3}), even if fluorescence is dominant, collisional de-excitation of the H_2 molecule must be taken into account; the spectrum is modified and approaches the thermal spectrum seen, for example, in shocked regions.

Fig. 7(a) shows (2,1) S(1) 2.247 μm/(1,0) S(1) 2.212 μm plotted against (1,0) S(2) 2.033 μm/(1,0) S(0) 2.223 μm. The models of Mouri (1994) are also reproduced. This plot confirms the trend already observed in Paper I: most AGNs (full circles, this work; open squares, Paper I) are distributed around the thermal curve, with excitation temperatures for the thermal component between 1500 and 2500 K. For these galaxies, the H_2 emission is dominated by thermal excitation. For a few objects, a mixture of thermal and non-thermal processes are at work, with the excitation temperature of the thermal component higher than 1000 K. Note that the fraction to which the non-thermal emission contributes to the H_2 emission is not larger than 30 per cent, as can be inferred from the predicted line ratios of the mix model (mixture of thermal and non-thermal models) also plotted in Fig. 7 (triangles). Regardless of their type (Seyfert I or Seyfert II), AGNs are concentrated in the upper-left portion of the figure. Note that heating by UV radiation (i.e. PDRs) points with H_2 2.033 μm/2.223 μm ~ 1 seems to play a minor role, except in a few objects, all of them with known starburst activity. We have also added to Fig. 7 the predictions of models of X-ray heating (open triangles) of Lepp & McCray (1983). As can be seen, they occupy the upper-left portion above the thermal curve, very close to the region where NGC 34, Mrk 573, MCG–5–13–17, NGC 5953 and ESO 428-G014 are located. This suggests that X-ray heating is a likely source of H_2 excitation for these objects. We do not discard the possibility that an additional parameter such as the density of the ionization parameter may play a role in order to explain the points far above the thermal curve. However, it is not possible to confirm this from our data. Overall, it can be stated that the bulk of H_2 in AGNs is powered by thermal excitation (either shocks or X-ray heating). Although Fig. 7 does not allow us to distinguish between these two mechanisms, additional observational evidence will be employed in the following sections to address this issue.

Previous studies carried out in smaller samples of AGNs have reached conflicting conclusions. Reunanen et al. (2002, 2003) found, for a sample of 14 AGNs (four of their objects common to this work), that the nuclear H_2 was mostly thermal emission, very likely associated with heating by X-rays. Using *Infrared Space Observatory* (*ISO*) observations of 13 starburst galaxies and nine AGNs (two of their objects common to our sample), Rigolopoulou et al. (2002) proposed that very likely a combination of emission from photodissociation regions, shock emission and gas heated by X-rays (mostly for the Seyferts) are responsible for H_2 excitation in extragalactic environments. Note that the large *ISO* apertures relative to that used in our data prevents a reliable comparison between the line fluxes. The results reported here agree with the above results, supporting the hypothesis that the molecular hydrogen is most likely associated with the AGN rather than star-forming activity. In contrast, very recently, Davies et al. (2005) have reported Very Large Telescope (VLT) ISAAC *K*-band spectroscopy of nine galaxies hosting an AGN, aimed at investigating the origin of the H_2 excitation. Their results suggest that the H_2 emission arises mostly in dense clouds illuminated by intense far-ultraviolet (FUV) radiation and consider unlikely that the AGN is the dominant source of excitation for the NIR H_2 emission. The above shows that, undoubtedly, more detailed work on a selected sample of objects at subarsec resolution and three-dimensional spectroscopy is needed in order to set further constrains on this issue.

Fig. 7(b) shows H_2 (2–1) S(1) 2.247 μm/(1,0) S(1) 2.212 μm versus H_2 (1–0) S(3) 1.963 μm/(1–0) S(1) 2.212 μm; this is an additional diagnostic diagram proposed by Mouri (1994), equivalent to that of Fig. 7(a). However, it has the drawback of including H_2 (1–0) S(3) 1.957 μm, which may be strongly affected by telluric absorption bands of H_2O and CO_2. This additional diagram supports the conclusions already drawn: most AGNs show a dominance of thermal processes over non-thermal processes, with thermal excitation temperature in the range 1000–3000 K.

4.1 Excitation temperatures and masses for H_2

An alternative way of confirming the results found in the previous section is to derive the rotational and vibrational temperatures for the molecular H_2 gas; thermal excitation must give similar rotational and vibrational temperatures, as would be expected for a gas in local thermodynamic equilibrium. Fluorescent excitation, on the other hand, is characterized by a high vibrational temperature and a low rotational temperature; non-local UV photons, not characteristic of the local kinetic temperature, overpopulate the highest energy levels compared to that expected for a Maxwell–Boltzmann population.

The values of T_{vib} and T_{rot} found for the galaxy sample are listed in Table 4. They were calculated using the fluxes of the observed H_2

Table 3. Fluxes of atomic and molecular lines, in units of 10^{-15} erg cm^{-2} s^{-1}, measured in the sample.

Galaxy	[Fe II] (1.257 μm)	Paβ (1.2820 μm)	[Fe II] (1.644 μm)	H_2 (1–0) S(3) (1.957 μm)	H_2 (1–0) S(2) (2.0332 μm)	H_2 (1–0) S(1) (2.1213 μm)	H_2 (1–0) S(0) (2.223 μm)	H_2 (2–1) S(1) (2.247 μm)	Brγ (2.165 μm)	1.257 μm/ 1.644 μm
Mrk 334	8.45±0.21	14.68±0.55[a]	6.10±0.29	3.80±0.23	1.35±0.08	2.72±0.17	<0.51	<0.33	4.69±0.15[c]	1.38±0.06
NGC 34	13.76±1.24	12.83±1.13	11.00±2.87	12.43±1.02	4.66±0.23	12.15±1.27	<2.13	<0.73	7.12±0.13	1.25±0.30
NGC 262	11.59±0.52	10.75±0.33	9.09±0.31	2.09±0.18	0.60±0.09	1.61±0.05	<0.25	<0.13	1.09±0.11	1.27±0.06
Mrk 993	5.05±0.30	14.90±2.66	–	1.63±0.10	0.92±0.12	1.01±0.17	<0.40	<0.26	<0.19	–
NGC 591	17.19±0.75	15.14±0.49	14.19±0.73	6.82±0.63	2.66±0.22	6.52±0.14	1.77±0.16	0.70±0.16	3.55±0.22	1.21±0.07
Mrk 573	5.90±0.14	9.58±0.17	4.11±0.09	1.44±0.17	0.75±0.24	1.82±0.19	<0.37	<0.10	2.77±0.09	1.44±0.04
NGC 1097	–	–	–	6.57±0.64	2.22±0.35	3.89±1.16	<0.71	< 0.21	–	–
NGC 1144	0.91±0.23	<0.14	–	<0.39	0.47±0.06	0.94±0.04	<0.26	<0.09	<0.14	–
Mrk 1066	38.53±0.25	54.07±0.24	37.07±0.34	15.17±0.38	4.83±0.10	13.41±0.16	2.66±0.06	1.77±0.03	14.16±0.22	1.03±0.01
NGC 1275	63.49±1.51	60.66±3.15	61.49±0.65	43.15±0.67	15.26±0.33	42.95±0.37	11.81±0.30	4.51±0.33	9.77±0.41	1.03±0.03
NGC 1614	35.02±1.22	129.28±1.14	20.84±2.91	11.18±3.97	<0.26	5.70±0.77	<0.45	<0.34	42.45±0.74	1.25±0.16
MCG–05–13–017	4.84±0.21	2.14±0.65[a]	–	2.88±0.36	0.59±0.12	2.04±0.10	<0.28	<0.07	0.78±0.06[b]	-
NGC 2110	81.24±1.02	14.91±0.86	70.17±0.55	11.35±0.28	4.22±0.21	8.39±0.19	2.70±0.36	<0.78	2.50±0.22	1.16±0.01
ESO 428-G014	30.24±0.62	45.26±0.57	28.47±1.05	8.29±0.55	3.06±0.27	8.27±0.12	<1.14	<0.38	8.98±0.14	1.06±0.04
NGC 5929	8.44±0.36	7.68±0.20	7.83±0.37	3.07±0.60	1.33±0.23	2.88±0.22	0.80±0.26	<0.50	1.35±0.25	1.08±0.07
NGC 5953	19.06±0.66	<5.44	15.21±1.89	6.67±1.85[d]	2.28±0.72	3.54±0.51	<1.10	<0.08	<2.77	1.25±0.14
Arp 102B	9.66±0.81	–	7.25±0.41	1.71±0.20	0.66±0.11	1.77±0.16	0.31±0.09	<0.17	–	1.33±0.12
ARK 564	3.91±0.29	43.16±0.45[a]	2.89±0.30	0.92±0.22	0.53±0.18	1.18±0.10	<0.22	<0.16	4.76±0.16[a]	1.35±0.15
NGC 7469	12.44±0.69	31.66±1.74[a]	9.87±0.68	16.04±0.61	3.28±0.23	8.74±0.28	2.02±0.53	1.55±0.53	4.52±0.28[a]	1.26±0.10
NGC 7674	10.81±0.92	10.36±0.58	9.74±0.47	4.05±0.56	1.20±0.23	2.12±0.12	0.67±0.11	<0.17	3.13±0.25	1.11±0.10
NGC 7682	4.58±0.74	9.92±0.65	–	9.40±0.51	3.50±0.22	9.78±0.14	2.51±0.30	<0.44	1.94±0.11	–
NGC 7714	17.35±0.53	59.73±1.38	14.84±2.08	<0.55	<0.30	3.31±0.43	<0.75	<0.38	15.47±0.28	1.17±0.15

[a]Narrow component. [b]Total flux. [c]Total flux. Line without broad component. [d]Strongly affected by telluric absorption.

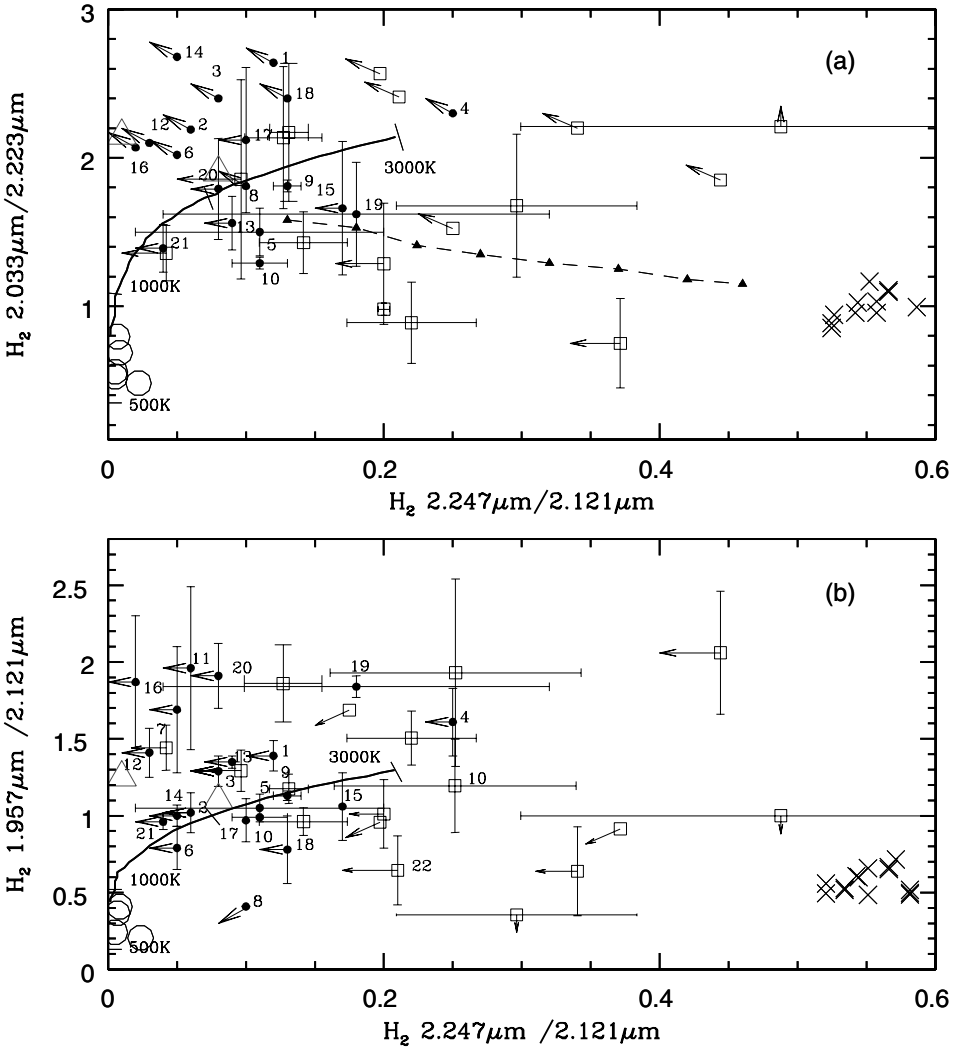

Figure 7. Plot of (a) (2–1) S(1) 2.247 μm/(1–0) S(1) 2.121 μm versus (1–0) S(2) 2.033 μm/(1–0) S(0) 2.223 μm and (b) (2–1) S(1) 2.247 μm/(1–0) S(1) 2.121 μm versus (1–0) S(3) 1.957 μm/(1–0) S(1) 2.121 μm. Curves represent thermal emission at 500–3000 K. Crosses are the non-thermal UV excitation models of Black & van Dishoeck (1987). Objects listed in Table 1 are represented by full circles while open squares denote the sample described in Paper I. Open circles are thermal UV excitation models of Sternberg & Dalgarno (1989) and open triangles are thermal X-ray models of Lepp & McCray (1983). The numbers identify each object according to the notation given in column 1 of Table 1. The full triangles, joined by a dashed line, represent the predicted line ratios from a mixture of thermal and low-density fluorescence models of Black & van Dishoeck (1987). The percentage of the thermal component decreases in steps of 10 per cent (and consequently the non-thermal component increases by the same proportion), starting from a model where 90 per cent is thermal and 10 per cent UV fluorescence (the first triangle from left to right) up to a contribution of 20 per cent thermal and 80 per cent non-thermal (last triangle of the sequence, to the right).

lines listed in Table 3 and the expressions $T_{\rm vib} \cong 5600/\ln(1.355 \times I_{1-0\,S(1)}/I_{2-1\,S(1)})$ and $T_{\rm rot} \cong -1113/\ln(0.323 \times I_{1-0\,S(2)}/I_{1-0\,S(0)})$ from Reunanen et al. (2002). Note that only for a small subsample of targets could we derive both temperatures accurately while, for most objects, upper limits to these quantities were calculated. It can be seen that $T_{\rm vib}$ and $T_{\rm rot}$ tend to be similar, although large discrepancies are noted in some objects. On average, we found that $T_{\rm vib} =$ 2050 K and $T_{\rm rot} = 2200$ K, including upper limits. This result gives additional support to thermal excitation as the driving mechanism for H_2 emission, with the temperatures ∼2000 K. Moreover, no statistical differences between the values found for Seyfert 1s (Paper I) and Seyfert 2s (this work) as well as to those derived by Reunanen et al. (2002) are observed. The temperatures listed in Table 4 point out that in Mrk 573, NGC 1614 and 7714, heating by UV photons, most probably associated with star-forming regions, is the main source of H_2 excitation. This is in accord with the nature of these three galaxies: they all have a strong starburst activity in the circumnuclear region.

In addition to the temperature, the fluxes of Table 3 allow us to derive the corresponding mass of hot H_2 emitting the 1–0 S(1) 2.121 μm line by means of the equation

$$m_{\rm H_2} \simeq 5.0875 \times 10^{13} D^2 I_{1-0\,S(1)}$$

taken from Reunanen et al. (2002) and assuming $T = 2000$ K, a transition probability $A_{S(1)} = 3.47 \times 10^{-7}$ s^{-1} (Turner, Kirby-Docken & Dalgarno 1977) and the population fraction in the $v = 1$, $J = 3$ level $f_{v=1,J=3} = 0.0122$ (Scoville et al. 1982). Note that in the above expression, $I_{1-0\,S(1)}$ is the flux of H_2 2.121 μm corrected by intrinsic $E(B–V)$. Table 5 lists the mass of molecular gas derived for the galaxies of this work and Paper I (column 4). Column 2

Table 4. Vibrational and rotational temperatures (in units of K) found for the molecular hydrogen in the galaxy sample.

Galaxy	T_{vib}	T_{rot}	Galaxy	T_{vib}	T_{rot}
Mrk 334	<2300	–	MCG–05–13–017	<1600	<1000
NGC 34	<1800	<3200	NGC 2110	<1500	3500±500
NGC 262	<2000	<4400	ESO 428-G014	<1700	–
Mrk 993	<3400	<3800	NGC 5929	<2200	1100±200
NGC 591	2200±100	1600±200	NGC 5953	<1400	<2800
Mrk 573	<1800	<600	Arp 102B	<2100	3000±2300
NGC 1097	<1800	–	ARK 564	<2500	<4500
NGC 1144	<2100	<2100	NGC 7469	2800±200	1800±600
Mrk 1066	2400±100	2100±100	NGC 7674	<1700	2100±700
NGC 1275	2200±100	1300±100	NGC 7682	<1500	1500±200
NGC 1614	<1800	<700	NGC 7714	<2300	<600

Table 5. Reddening corrected H_2 fluxes masses calculated for the nuclear molecular gas. The galaxies of Paper I are also included in this list.

Galaxy	$E(B-V)$ (mag)	$F_{2.121\ \mu m}$ $\times 10^{-15}$ erg cm^{-2} s^{-1}	Mass ($M_\odot$)
Mrk 334	0.70	5.10	2000
NGC 34	1.32	39.47	12 600
NGC 591	0.36	8.98	1700
Mrk 573	0.59	3.09	700
NGC 1144	1.97	5.49	3700
Mrk 1066	0.48	20.62	2400
NGC 1614	0.73	10.98	2300
MCG–05–13–17	0.85	4.36	600
ESO 428G	0.17	9.64	300
NGC 5929	0.04	2.98	200
NGC 5953	1.22	10.56	400
NGC 7674	0.64	3.76	2600
NGC 7682	0.16	11.24	2700
NGC 7714	0.47	5.03	400
Mrk 1210	0.13	2.25	400
NGC 3227	0.61	30.61	400
NGC 3310	0.76	3.04	30
NGC 4151	0.32	19.61	200
Mrk 766	0.52	3.78	500
NGC 5548	0.57	1.34	300
NGC 5728	0.58	10.55	900
NGC 262	0	0.96	300
NGC 4748	0	1.48	300
Mrk 1239	0	0.37	<200
NGC 7469	0	7.34	1900
NGC 2110	0	8.27	400
NGC 1275	0	40.68	10 800
Mrk 993	0	0.08	200

lists the value of $E(B-V)$ used to correct the observed H_2 2.121 μm flux. It was calculated from the flux ratio Paβ/Brγ, assuming an intrinsic value of 5.88 following the case B (Osterbrock 1989), and the extinction law of Cardelli, Clayton & Mathis (1989). For Seyfert 1 galaxies, we used the fluxes of the narrow components only. Those objects where a deblending was not possible or it was highly uncertain were left out of the calculation. Column 3 of Table 5 lists the H_2 2.121 μm reddened corrected flux.

Except for two objects (NGC 34 and 1275), where we found that the mass of H_2 is larger than 10^4 $M_\odot$ (12 600 and 10 800 $M_\odot$, respectively) the mass of hot molecular hydrogen emitting H_2 2.121 μm is scattered over one order of magnitude (10^2–10^3 $M_\odot$), with 75 per cent of the AGNs displaying masses smaller than 2×10^3 $M_\odot$. These figures are also in very good agreement with those derived by Reunanen et al. (2002, 2003) and Rigolopoulou et al. (2002) for other AGNs. Moreover, no difference in mass is observed between Seyfert 1s and Seyfert 2s, as can be seen in Fig. 8, where a histogram for the distribution of H_2 masses for Seyfert 1s (full line) and Seyfert 2s (dashed line) is drawn. Note that for visualization purposes, the two outliers noted above were left out of the plot.

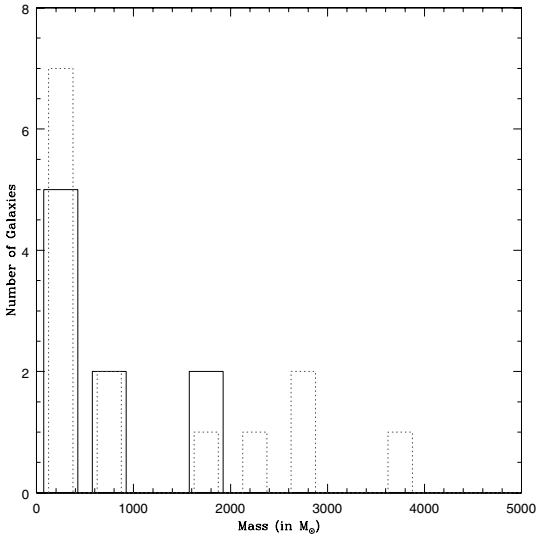

Figure 8. Molecular mass distribution for the AGN sample. Seyfert 1s are shown by the full histogram. The dashed line is for Seyfert 2s. The bin size of the mass is 500 $M_\odot$.

The large similarity in the physical conditions and properties of the molecular gas for such a large number of objects can be taken as evidence of the crucial role that the AGNs should play in the excitation of the H_2 gas. Since not all objects have a radio-jet or a circumnuclear starburst region, shocks, created in these two environments, would probably play a secondary role in the excitation of molecular gas. X-rays emitted by the AGN, on the other hand, are the common characteristic in all these objects. Therefore, heating by this radiation is suggested as the primary source of H_2 excitation. Note that, in Paper I, it was shown by means of X-rays models that this excitation mechanism can adequately reproduce the

observed H_2 and part of the [Fe II] fluxes. Because of the relatively small aperture used in the extraction of most spectra ($\leqslant$250 pc), the H_2 fluxes used in this work and in Paper I can be taken as truly representative of the nuclear region. This represents an advance over previous works (i.e. Rigolopoulou et al. 2002), where the large *ISO* apertures, of several arcsec, can dilute the effects of a pure-AGN related effect.

In order to explore the influence of X-rays in the observed molecular fluxes, we searched for a correlation between the intrinsic hard X-ray luminosity $L_{2-10\,\mathrm{keV}}$ versus the line ratio H_2 2.247 μm/2.121 μm. The hard X-ray data were taken from table 1 of Lutz et al. (2004), which is a compilation of data from many satellites (e.g. *ASCA*, *BeppoSAX*, *Chandra*, *XMM*). We found that no correlation exists between these two quantities. Note, however, that this result does not necessarily means that X-rays have little influence in the H_2 emission. This is because, for ratios larger than 0.2, the fraction of H_2 gas that is excited by fluorescence (where X-rays have no influence at all) increases appreciably. Note that the X-ray models plotted in Fig. 7 in fact suggest that X-rays play an important role in the molecular hydrogen excitation. A possible explanation for the lack of correlation is the similarity and small values of the masses of hot molecular gas in the objects of our sample. In this scenario, the H_2 emission would be matter-bounded.

In summary, the observational evidence presented using a sample of 44 AGNs shows that the molecular hydrogen lines in these objects are mostly thermal, with a contribution of non-thermal processes typically varying from 15 to 30 per cent. There is not, however, a unique process associated with the thermal component, with shocks, X-rays and UV heating being the main processes contributing to H_2 excitation.

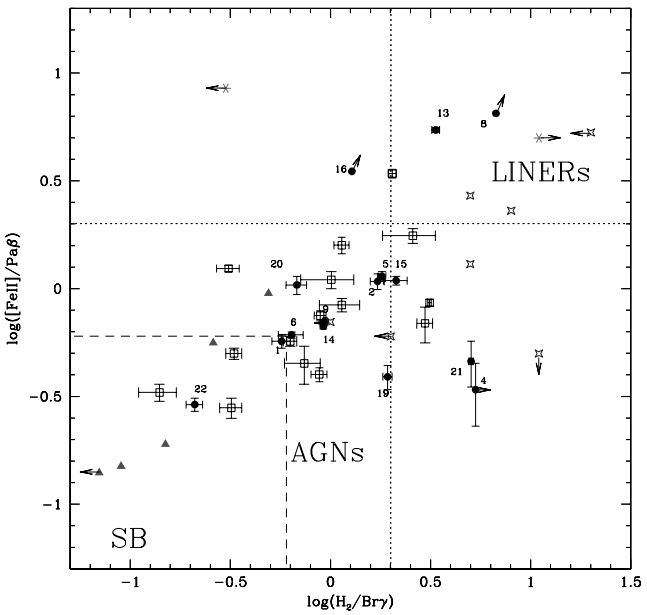

Figure 9. The ratios H_2 2.121 μm/Brγ and [Fe II] 1.257 μm/Paβ. Objects of this paper are plotted as full circles, and those of Paper I are represented by open squares. Triangles are starburst/H II of Dale et al. (2004) and Larkin et al. (1998), open stars are LINERs from (Larkin et al. 1998) and asterisks are supernova remnants, also taken from (Larkin et al. 1998). See text for further details. The number along each data point identifies the galaxies of our sample (this paper) according to the notation given in column 1 of Table 1.

5 TOWARDS A DIAGNOSTIC DIAGRAM FOR EMISSION-LINE OBJECTS IN THE NEAR-INFRARED

Based on the results obtained in the previous section and the fact that H_2 and [Fe II] lines are common features in the spectra of AGNs, it is interesting to investigate how these lines compare to other objects in which they are also present but have a different degree of nuclear activity. As we already know, the line ratios among H_2 lines in AGNs are distributed in a rather small range of values. This is the case of H_2 2.247 μm/2.121 μm, for instance, which ranges between 0.1 and 0.25. A similar comparison can also be made for [Fe II].

In Paper I, it was shown that the line ratios H_2 2.121 μm/Brγ and [Fe II] 1.257 μm/Paβ were suitable to separate emission-line objects according to their level of activity. Galaxies for which either one of the ratios was smaller than 2 were predominantly classified as Seyfert galaxies. Moreover, starburst galaxies were preferentially located in the region with [Fe II]/Paβ and H_2/Brγ < 0.4, while LINERs were characterized by [Fe II]/Paβ and H_2/Brγ ratios >2. However, the lack of an adequate number of Seyfert 2 objects in Paper I prevented us from making definitive conclusions. Here, with the augmented sample and, most importantly, the inclusion of Seyfert 2s, we are in a position to confirm the trend already observed.

Fig. 9 shows H_2 2.121 μm/Brγ versus [Fe II] 1.257 μm/Paβ. The sample of objects analysed in this work is represented by full circles while objects of Paper I are represented by open squares. Triangles represent line ratios gathered from the starburst sample of Dale et al. (2004) and Larkin et al. (1998), open stars are LINERs and crosses are supernova remnants, the latter two sets of measurements gathered from Larkin et al. (1998).

It can be seen that the trend previously suggested is confirmed: AGNs are characterized by H_2 2.121 μm/Brγ and [Fe II] 1.257 μm/Paβ flux ratios between 0.6 and 2. Starburst/H II galaxies display line ratios <0.6 while LINERs are characterized by values larger than 2 in either ratio.

The plot shown in Fig. 9 represents the most updated and completed version of this diagram made up to date. In a study of LINERs and other emission-line objects, including a few Seyferts, Larkin et al. (1998) reported a strong linear correlation in the log–log space between [Fe II]/Paβ and H_2/Brγ, with LINERs displaying the largest ratios, starburst galaxies the smallest ratios and Seyferts intermediate values. They suggested that [Fe II]/Paβ $\sim$1 and H_2/Brγ $\sim$3 mark the end of Seyfert-like nuclei and the beginning of LINER-like objects. With our sample of points, comprising 28 AGNs, we not only confirm Fig. 9 as a suitable means of separating emission-line objects by their degree of activity in the NIR region, but also we propose that both H_2/Brγ and [Fe II]/Paβ in AGNs preferentially display values in either ratio <2.

The diagnostic diagram of Fig. 9 arises as an important and a very efficient tool in the NIR for classifying emission-line objects according to their nuclear level of activity. Although similar diagrams exist in the optical region (i.e. [N II] λ6584/Hα versus [O III] λ5007/Hβ; Veilleux & Osterbrock 1987), where AGNs are clearly separated from LINERs, starburst and H II galaxies, it fails for objects with $A_v \geqslant 3$, that is, for galaxies with buried AGNs. Although one can argue that in the NIR AGNs can be unambiguously distinguished from other emission-line objects by the detection of coronal lines (i.e. [Si VI] 1.963 μm, [Ca VIII] 2.321 μm), not all AGNs display such high ionization lines. In our sample, for instance, only 10 out of 19 AGNs show signatures of [Si VI] and [Ca VIII]. In addition, the latter line was only detected in a handful of objects and usually is severely hidden by the CO band-heads at 2.3 μm. Moreover, in

the *K* band, both [Si VI] and [Ca VIII] are located in regions strongly affected by telluric features, preventing their use as diagnostics in objects with poor signal-to noise.

Interestingly, NGC 3998 and 4826, two of the objects cataloged by Larkin et al. (1998) as LINERs and which appear in Fig. 9 in the region populated mostly by AGNs, are in fact AGN-like objects. The detection of broad Hα in the spectrum of the former (Ho et al. 1997) and a classification of the latter as a Seyfert 2 give additional support to the usefulness of this diagnostic diagram.

On a pure observational basis, the interpretation of Fig. 9 is not straightforward. One can argue that the correlation observed between $H_2/Br\gamma$ and [Fe II]/Paβ is due to the fact that both H_2 and [Fe II] are excited by the same mechanism, i.e. X-ray heating. However, this is a plausible explanation, as was discussed in Sections 4 and 4.1, for AGNs and, to a much lower extent, for LINERs. In fact, Larkin et al. (1998) argue that hard X-ray heating from a power-law source is a plausible mechanism to explain LINERs with low values of the [Fe II]/Paβ and H_2 2.121 μm/Brγ ratios. However, it would not explain the high values, of up to ∼7, observed in some objects.

The fact that the spectra of supernova remnants display high values of [Fe II]/Paβ while those of star-forming regions are characterized by low values of that ratio makes attractive the hypothesis that in some LINERs the high [Fe II]/Paβ ratio is primarily driven by shocks produced in these remnants (Larkin et al. 1998). Low values of [Fe II]/Paβ, on the other hand, would be the results of objects powered by star formation, as is the case of starburst/H II galaxies. In this regard, the [Fe II]/Paβ ratio is a measure of the star formation history of the galaxy, being low in objects ionized by young massive stars and large in objects in which the burst of star formation is in the final stage of processing (i.e. LINERs). This scenario is, in fact, supported by Alonso-Herrero et al. (2000) by means of *J* and *H* spectroscopy on a sample of LINERs. They claimed that the emission-line properties of many LINERs can be explained in terms of an ageing starburst, which they modelled in terms of a metal-rich H II region plus a supernova remnant component. The proportions of the two components are set by the [Fe II]/Paβ line ratio and would make an object appear either at the upper-right corner ([Fe II] due to supernova remnant driven shocks) or at the bottom-left corner ([Fe II] due to massive young stars). The location of AGNs (X-ray heating), in between these two extremes, is not clear in this scenario but very likely is the result of a power-law continuum illuminating a slab of gas.

It is yet possible that an AGN displays large values of the [Fe II]/Paβ ratio (larger than 2), making it appear as a LINER according to its position in the diagram, but with [Fe II] unrelated to supernova shocks. Shocks produced by the interaction between a radio jet and the NLR gas can be the primary source of heating, exciting the [Fe II] ions, for example. This would be the case of NGC 2110. In spite of being a Seyfert 2 galaxy, its position in Fig. 9 is more compatible with a LINER-like nucleus rather than a Seyfert-like object. *Hubble Space Telescope* imaging and spectroscopy on this source reveal both a narrow, 1-arcsec-long jet/region of [O III] emission extending to the north of the nucleus. Moreover, early radio observations found NGC 2110 to be a strong radio source (Bradt et al. 1978) and subsequent Very Large Array (VLA) imaging (Ulvestad & Wilson 1983, 1984) showed symmetrical, jet-like radio emission, extending 4 arcsec in the north–south direction and straddling a central compact core. Note that the hard X-ray luminosity of NGC 2110 is comparable to those of Seyfert 1 galaxies (Weaver et al. 1995; Malaguti et al. 1999). This means that for some AGNs, it is possible to have two sources of [Fe II] and their competing effect can define their position in Fig. 9. As our data show, this seems to be a special case and in no way affects the usefulness of Fig. 9 discussed above.

6 FINAL REMARKS

In order to discuss the origin of the molecular hydrogen and [Fe II] emission lines, NIR observations have been carried out for a sample of six Seyfert 1 galaxies, 15 Seyfert 2 galaxies and one H II galaxy. These data are complemented by 21 AGNs and one starburst galaxy analysed in a former publication (Paper I). The whole set of data constitutes the most complete and homogeneous sample of AGNs observed in the NIR to date. Our main conclusions are briefly reviewed.

The kinematic link between the molecular hydrogen and the NLR gas was analysed on the basis of the linewidths. The observational evidence confirms that H_2 is common within the inner few hundred parsec of an AGN, regardless of its type. However, the molecular gas follows a different kinematics than that of the classical NLR gas, as can be inferred from the large differences in linewidth between the molecular lines and that of the NLR. Rotation curves derived for H_2 and published by other authors for objects that are common to our sample supports this hypothesis and points to a scenario where a disc of H_2 surrounds the nuclear region. It is then unlikely that H_2 and [Fe II] come from the same volume of gas.

Emission-line ratios of H_2 that discriminate between thermal and fluorescence excitation show that in AGNs the excitation mechanism is clearly thermal with a contribution of non-thermal processes of up to 30 per cent. This result is further supported by the similarity between the vibrational and rotational temperatures of H_2 in some objects and the tendency of $T_{\rm vib}$ to be larger than $T_{\rm rot}$ in others. The latter fact can be due to X-ray excitation, which would favour vibrational transitions over rotational transitions due to the larger energies involved in the former than in the latter. The mass of hot molecular gas emitting the H_2 lines ranges from 10^2 to 10^3 $M_\odot$, with nearly half of the objects showing values of <500 $M_\odot$. No differences are observed either in temperature or in mass values between Seyfert 1s and Seyfert 2s, in accord with the unified model of AGNs. Based on the fact that neither radio jets nor a starburst component are common characteristics in all AGNs of our sample, we conclude that X-ray heating should be the main excitation mechanism of H_2.

We have confirmed that the diagram involving the line flux ratios H_2 2.121 μm/Brγ and [Fe II] 1.257 μm/Paβ is an efficient tool for separating emission-line objects according to their dominant degree of activity and should be useful for classifying objects with hidden AGNs or highly reddened objects. We have found that AGNs are characterized by H_2 2.121 μm/Brγ and [Fe II] 1.257 μm/Paβ flux ratios between 0.6 and 2. Starburst/H II galaxies display line ratios <0.6 while LINERs are characterized by values larger than 2 in either ratio. The positive correlation found between the above ratios is more likely apparent since different mechanisms drive the production of either [Fe II] or H_2 according to the level of nuclear activity. It is not discarded that in AGNs a combination of X-ray heating from the central source and shock heating (produced by the jet–NLR gas interaction) can simultaneously drive the emission of [Fe II], making the AGN appear LINER-like. These cases, however, seem to be uncommon and do not affect the results presented here.

ACKNOWLEDGMENTS

This paper is partially supported by the Brazilian funding agency CNPq (309054/03-6) to ARA. This research has made use of the

NASA/IPAC Extragalactic Database (NED), which is operated by the Jet Propulsion Laboratory, California Institute of Technology, under contract with NASA.

REFERENCES

Alloin D., Galliano E., 2002, A&A, 393, 43
Alonso-Herrero A., Rieke M. J., Rieke G. H., Ruiz M., 1997, ApJ, 482, 747
Alonso-Herrero A., Rieke M. J., Rieke G. H., Shields J. C., 2000, ApJ, 530, 688
Antonucci R. R. J., Miller J. S., 1985, ApJ, 297, 621
Black J. H., van Dishoeck E. F., 1987, ApJ, 322, 412
Bradt H. V., Burke B. F., Canizares C. R., Greenfield P. E., Kelley R. L., McClintock J. E., Koski A. T., van Paradijs J., 1978, ApJ, 226, L111
Cardelli J. A., Clayton G. C., Mathis J. S., 1989, ApJ, 345, 245
Contini M., Radovich M., Rafanelli P., Richter G. M., 2002, ApJ, 572, 124
Cushing M. C., Vacca W. D., Rayner J. T., 2004, PASP, 116, 362
Dale D. A. et al., 2004, ApJ, 601, 813
Davies R. I., Sternberg A., Lehnert M. D., Tacconi-Garman L. E., 2005, ApJ, in press (astro-ph/0507062)
Forbes D. A., Ward M. J., 1993, ApJ, 416, 150
Goodrich R. W., Veilleux S., Hill G. J., 1994, ApJ, 422, 521
Gratadour D., Clénet Y., Rouan D., Lai O., Forveille T., 2003, A&A, 411, 335
Ho L. C., Filippenko A. V., Sargent W. L., Peng C. Y., 1997, ApJS, 112, 391
Hollenbach D., McKee C. F., 1989, ApJ, 342, 306
Ivanov V. D., Rieke G. H., Groppi C. E., Alonso-Herrero A., Rieke M. J., Engelbracht C. W., 2000, ApJ, 545, 190
Knop R. A., Armus L., Larkin J. E., Matthews K., Shupe D. L., Soifer B. T., 1996, AJ, 112, 81
Larkin J. E., Armus L., Knop R. A., Soifer B. T., Matthews K., 1998, ApJS, 114, 59
Lepp S., McCray R., 1983, ApJ, 269, 560
Lutz D., Maiolino R., Spoon H. W. W., Moorwood A. F. M., 2004, A&A, 418, 465
Malaguti G., Bassani L., Cappi M., Comastri A., di Cocco G., 1999, A&A, 342, L41
Maloney P. R., Hollenbach D. J., Tielens A. G. G. M., 1996, ApJ, 466, 561
Mouri H., 1994, ApJ, 427, 777
Mouri H., Kawara K., Taniguchi Y., 2000, ApJ, 528, 186
Osterbrock D. E., 1989, Astrophysics of Gaseous Nebulae and Galactic Nuclei. University Science Books, Mill Valley, CA
Quillen A. C., Alonso-Herrero A., Rieke M. J., Rieke G. H., Ruiz M., Kullarni V., 1999, ApJ, 527, 696
Rayner J. T., Toomey D. W., Onaka P. M., Denault A. J., Stahlberger W. E., Vacca W. D., Cushing M. C., Wang S., 2003, PASP, 155, 362
Reunanen J., Kotilainen J. K., Prieto M. A., 2002, MNRAS, 331, 154
Reunanen J., Kotilainen J. K., Prieto M. A., 2003, MNRAS, 343, 192
Rigolopoulou D., Kunze D., Lutz D., Genzel R., Moorwood A. F. M., 2002, A&A, 389, 374
Rodríguez-Ardila, Pastoriza M. G., Viegas S. M., Sigut T. A. A., Pradhan A. K., 2004, A&A, 425, 457 (Paper I)
Schinnerer E., Eckart A., Tacconi L. J., 1999, ApJ, 524, L5
Schlegel D. J., Finkbeiner D. P., Davis M., 1998, ApJ, 500, 525
Scoville N. Z., Hall D. N. B., Kleinmann S. G., Ridgway S. T., 1982, ApJ, 459, 535
Simpson C., Forbes D. A., Baker A. C., Ward M. J., 1996, MNRAS, 283, 777
Sternberg A., Dalgarno A., 1989, ApJ, 338, 197
Sturm E., Lutz D., Verma A., Netzer H., Sternberg A., Moorwood A. F. M., Oliva E., Genzel R., 2002, A&A, 393, 821
Turner J., Kirby-Docken K., Dalgarno A., 1977, ApJS, 35, 281
Ulvestad J. S., Wilson A. S., 1983, ApJ, 264, L7
Ulvestad J. S., Wilson A. S., 1984, ApJ, 285, 439
Vacca W. D., Cushing M. C., Rayner J. T., 2003, PASP, 155, 389
Veilleux S., Osterbrock D. E., 1987, ApJS, 63, 295
Veilleux S., Goodrich R. W., Hill G. J., 1997a, ApJ, 477, 631
Weaver K. A., Mushotzky R. F., Serlemitsos P. J., Wilson A. S., Elvis M., Briel U., 1995, ApJ, 442, 597

This paper has been typeset from a TEX/LATEX file prepared by the author.